JOURNAL OF THERMOPHYSICS AND HEAT TRANSFER
Vol. 22, No. 3, July–September 2008

Unsteady Numerical Investigation of Blade Tip Leakage, Part 1: Time-Averaged Results

Patricia Phutthavong* and Ibrahim Hassan†
Concordia University, Montreal, Quebec H3G 1M8, Canada
and
Terry Lucas‡
Pratt and Whitney Canada, Longueuil, Quebec J4G 1A1, Canada

DOI: 10.2514/1.29312

In today's modern gas turbine engines, the region between the rotor and the stationary shroud has the most extreme fluid-thermal conditions in the entire turbine and is characterized by a periodically unsteady three-dimensional flowfield. The purpose of the present work is to conduct an unsteady study of the tip leakage flow adjacent to the shroud in real gas turbine engines using an in-house industrial computational fluid dynamics code. Both time-averaged and time-dependent data for the velocity, temperature, and mass flow rate in the tip clearance region are presented in parts 1 and 2, respectively. In part 1, it was found that near the pressure side of the tip clearance region and near the blade tip on the suction side, the leakage flow is dominant, whereas opposing flows entering through the suction side dominate near the shroud and at the suction side. This opposing flow is the combined effect of the shroud relative motion and the crossflow originating from the adjacent blade passage on the suction side. A small recirculation region was observed above the rotor passage and was attributed to the blade-passage crossflow interacting with the high-pressure region found at the suction side of the blade. This high-pressure region is caused by the combined effect of the crossflow with the shroud boundary-layer flow interacting with the tip leakage flow inside the tip clearance region.

Nomenclature

b	=	blade span
C_x	=	blade axial chord
h	=	tip clearance height
M	=	Mach number
P	=	pressure
r	=	radial coordinate
T	=	temperature
$\boldsymbol{v}$	=	velocity vector
W	=	mass flow rate
x	=	axial coordinate
y	=	Cartesian coordinate oriented along the circumferential direction
z	=	Cartesian coordinate oriented along the radial direction

Subscripts

aw	=	adiabatic wall
c	=	core flow
o	=	stagnation properties
rel	=	relative
s	=	isentropic

I. Introduction

IN MODERN gas turbine engines, tip clearances between rotating turbine blades and stationary shrouds are very small, and in some cases, they are even smaller than 1 mm in height. The shroud over a turbine rotor is exposed to intense heat conditions, and it is important to be able to predict heat transfer coefficients in the tip gap region to optimize the amount of shroud cooling so that the performance does not suffer too great a loss. The rapid development of high-temperature turbines has vastly surpassed the fundamental research of the thermal field in the tip clearance region between the shroud and the rotor. In the first turbine stage, the transitional region between the rotor and the stationary shroud has the most extreme fluid-thermal conditions in the entire turbine and is characterized by a periodically unsteady three-dimensional flowfield. Therefore, it is very difficult to accurately represent the flow phenomena analytically.

The heat transfer in the blade tip gap region of modern gas turbine engines is driven by the extremely complex tip gap flowfield. Tip leakage flow consists of hot mainstream gas and is highly undesirable because it does not turn and so does not produce any work. Also, high heat transfer rates in the tip gap region occur as a result of leakage flow due to the formation of very thin boundary layers. In a gas turbine engine, the shroud is stationary while the rotor rotates beneath it, as seen from the absolute reference frame. Therefore, in the relative reference frame of the rotor, the shroud appears to be traveling above, from the suction side to the pressure side. The shroud's relative motion is opposite to the direction of the tip leakage flow, and so there is a stagnation line spanning from the pressure side to the suction side, where the flow velocity is zero in the tip gap region. In addition, a separation bubble develops on the pressure side of the blade tip as the leakage flow enters the tip gap region, due to the sudden change of curvature as the flow moves radially upward along the pressure side of the airfoil and into the tip clearance region. The leakage flow leaves the suction side of the blade tip in the form of a vortex as it comes in contact with crossflow. The subsequent mixing of the leakage flow with the main flow causes the momentum of main passage flow to decrease, further decreasing the efficiency of the engine.

Today's advanced experimental and numerical techniques have allowed researchers to gain further insight into the loss mechanisms

Received 14 December 2006; revision received 6 October 2007; accepted for publication 18 October 2007.

*M.A.Sc. Student, Department of Mechanical and Industrial Engineering.
†Associate Professor, Department of Mechanical and Industrial Engineering, 1455 de Maisonneuve Boulevard West, Mailbox EV004.213; hassan@encs.concordia.ca (Corresponding Author).
‡Chief, Turbine Cooling and Static Structures, 1000 Marie-Victorin, Mailbox 01SA4.

arising in the tip gap region. However, it is still quite difficult to visualize tip gap flow in actual clearance gaps of real turbines, which can be smaller than 1 mm in height. In addition, most studies have been conducted at low speeds, which are not typical of the actual speeds found in gas turbine engines. Likewise, obtaining experimental measurements for heat transfer on the turbine shroud is extremely costly and difficult due to the high-temperature gradients as well as the size of the gap, as mentioned before. In the open literature, blade tip leakage flow has been studied over rotating blades [1–15]. In addition, tip leakage flow has been investigated over stationary airfoils [16–24]. Stationary cascades allow researchers to obtain detailed heat transfer data in this highly three-dimensional flow area between the rotor and shroud with relative ease. However, caution should be taken when applying these results to rotating turbines. Thus, the best alternative to field data is data from rotating turbine rigs, though it is important to note that these rigs operate with no combustion, which is somewhat unrealistic. In addition, simple models have been developed to describe the complex flowfield [5,10,17,25].

The summary of the literature review is as follows. Data from investigations with stationary cascades vary significantly from those with rotating blades, because the shroud's relative motion greatly affects the flowfield in the tip gap region. Leakage flow and thus the leakage vortex strength tend to be less in rotating blade studies because much of the leakage flow leaves the gap region, due to the obstruction caused by the shroud's boundary layer. Also, the opposing motion of the shroud on the tip leakage flow aids in reducing the tip leakage mass flow rate and momentum and causes the leakage vortex to remain near the suction side. In addition, the development of the tip leakage vortex is dependent on the size of the tip clearance: larger tip clearances allow for higher mass transfer rates and thus larger vortices. Although there are various simple models that have been generated over the years, a universal model of the complex flowfield in the blade tip gap has not yet been developed.

The ability to fully comprehend the mechanics behind the flow and heat transfer will enable engineers to design effective cooling schemes in these turbine components, because they are characterized by extreme thermal conditions that may lead to premature failure. Three-dimensional numerical simulations of the flow and heat transfer in the tip gap region are a less costly alternative to experiments and can potentially capture some flow behavior in areas in which measurement instrumentation cannot. From the review of the literature, no unsteady simulations have been conducted that focus on the flow structure inside the tip clearance region. This purpose of the present study is to conduct an unsteady numerical investigation of the flowfield in the tip clearance region of a typical gas turbine engine. In addition, a parametric study will be conducted to investigate the effect of tip clearance height, inlet turbulence intensity, inlet stagnation temperature, and rotor angular velocity on the flowfield in the tip clearance region.

II. Mathematical Modeling

The purpose of the present work is to study the effect of time variation on flow characteristics in the tip leakage region. Thus, unsteady simulations were conducted with both the stator and rotor modeled. To do so, multiple reference frames must be defined, because the stator flow domain is stationary, whereas the rotor flow domain rotates as time progresses. Also, a reliable steady-state solution is required as an initial solution for the unsteady simulations. For the unsteady simulations, sliding meshes were implemented for which the rotor mesh changes position at each time step, thus allowing for time-accurate solutions to be obtained.

The mixing-plane approach was used to obtain the required steady-state solution for the unsteady simulations. The main idea behind the mixing-plane approach is that each flow domain is solved as a steady-state problem. Here, circumferentially averaged flow data from adjacent flow domains are passed as boundary conditions at the mixing-plane interface. Thus, the spatially averaged profiles of flow data at the stator outlet will be the conditions for the rotor at its inlet. Any unsteadiness in the circumferential direction (such as wakes, shock waves, and separated flow) will be removed, thus yielding a steady-state time-averaged solution.

In summary, the solution algorithm for the mixing-plane approach is as follows:

1) Update the solution within the stator and rotor flow domains.

2) Compute the circumferentially averaged flow properties at the stator outlet and rotor inlet to obtain appropriate profiles.

3) Pass the profiles as boundary conditions at the mixing plane.

4) Repeat steps 1–3 until convergence.

The turbine stage, including the nozzle guide vane (NGV) and the rotor, will be modeled and simulated using a 3-D Reynolds-averaged Navier–Stokes finite volume code that is currently available in the aerospace industry. Description of the code may be found in [26–28]. The viscous grids generated by the code are structured meshes and provide y^+ values of less than 1 on all wall surfaces, which ensures that the SST k-ω turbulence model is being implemented correctly. In addition, all walls were considered to be adiabatic.

In the k-ω turbulence models, the wall boundary conditions for the k equation are accounted for through enhanced wall treatment, which are used in k-ε models. In the enhanced wall treatment, a two-layer model is combined with enhanced wall functions to model the flow near the wall. The enhanced thermal wall functions are determined using

$$T^+ = e^{\Gamma} T^+_{\text{lam}} + e^{\frac{1}{\Gamma}} T^+_{\text{turb}} \tag{1}$$

where

$$\Gamma = -\frac{a(Pry^+)^4}{1 + bPr^3 y^+} \tag{2}$$

with $a = 0.01$ and $b = 5$.

The NGV is modeled to obtain a realistic pressure distribution at the inlet of the rotor, which includes the effects of wakes originating in the NGV. Total pressure and total temperature were specified at the inlet of the vane domain, and static pressure was set at the outlet of the rotor domain. One vane passage and one rotor passage were modeled in the steady-state simulations, and one vane and two blade passages were modeled for the unsteady simulations. For the unsteady simulations, rotationally periodic boundary conditions were used to model the lowest number of vanes and blades such that the periodic angles of both the NGV and rotor are identical. The turbine stage under investigation in the present study consists of 30 vanes and 60 blades. Therefore, the computational domain for the unsteady simulations consists of one vane and two blades, yielding a periodic angle of 12 deg for both the NGV and rotor. A typical computational domain with both the NGV and rotor is shown in Fig. 1. Note that the blade tip is a flat blade tip, and its geometry was obtained through inference from figures that are available from the public literature.

In the present study, H meshes were used for both the vane and rotor domains, in which the number of nodes in the axial, circumferential, and radial directions of the domains were specified. The node count in the radial direction was set at 49, and the node counts in the axial and circumferential directions were varied such that the multigrid level was greater than three to ensure fast convergence of the solution. In addition, the node counts on the leading edge, the airfoil surface, and the trailing edge were also specified to accurately depict the shape of the airfoil. The code also generates a tip clearance region just above the blade tip in the rotor domain, with a node count of 16 in the radial direction. Thus, the total node count in the radial direction in the rotor domain was 65. For the unsteady simulations, a time step size of 1.05262×10^{-6} s was used, which is the time required such that 200 time steps are required to traverse one stator pitch of 12 deg, and 10 inner iterations per time step were used. For the Nistar code, 10 inner iterations are sufficient for the numerical residuals to decrease by two orders of magnitude.

It is important to note that the data were recorded on planes called the I planes, J planes, and K planes. Figure 2 shows the grid of a typical K plane in which I planes and J planes can be seen. As mentioned before, the meshes that are generated are structured and yield y^+ values of less than one. As a result, the meshes are very fine near the airfoil walls. Similarly, Fig. 3 shows a typical I plane, in

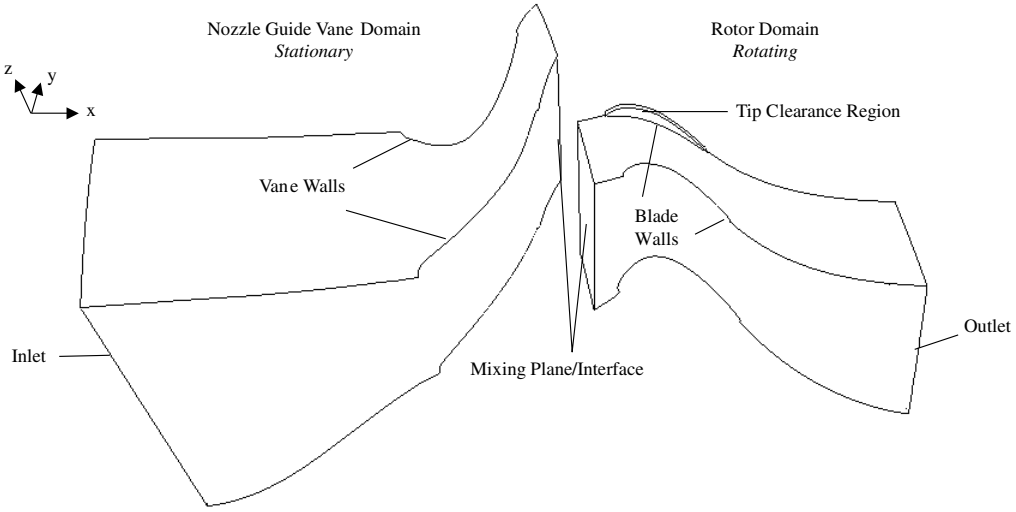

Fig. 1 Depiction of the NGV domain and rotor domain as modeled by Nistar.

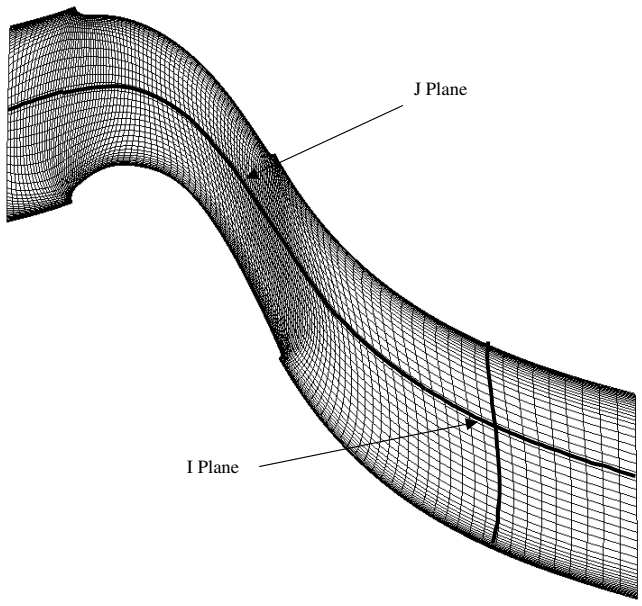

Fig. 2 Depiction of *I* and *J* planes on a typical *K* plane taken at midspan of the rotor domain.

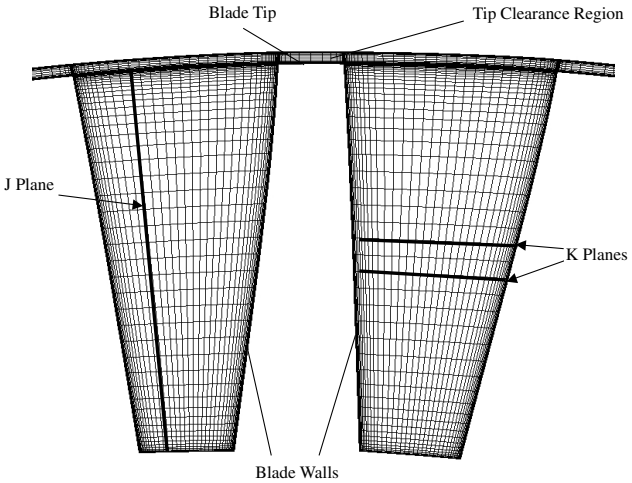

Fig. 3 Depiction of *J* and *K* planes on a typical *I* plane taken at midspan of the rotor domain.

which the tip clearance grid can also be seen. Once again, finer meshes can be seen close to the airfoil walls as well as the shroud. A node count of 49 was used in the radial direction, with an additional 16 nodes in the tip clearance region, which can be seen in Fig. 3. A grid independence test was conducted to determine the optimal node counts in the axial and circumferential directions and will be presented in the following section.

The convergence for the steady-state simulations was determined by assuring that the mass flow rates, the total pressure, and static pressure at the inlet and outlet of each domain remain constant over a large number of iterations. In the present study, the steady-state simulations were allowed to run for 5000 iterations. The converged steady-state solution was used as an initial solution for the unsteady simulations. For the unsteady simulations, it is important that the solution attains time periodicity before results are recorded. As a result, the simulation was allowed to run for 2000 time steps or 10 vane-passing periods, and the convergence parameters at the inlet and outlet of the domains were recorded to determine time periodicity.

III. Validation of Computational Fluid Dynamics Code

The time-averaged predictions of the experimental work of Chana and Jones [29] was used to validate the industrially owned computational fluid dynamics (CFD) code called Nistar. This work was chosen because the geometry of the turbine stage could be extracted and remodeled. In addition, results for the adiabatic-wall temperature on the shroud were reported by [29] and could be used to compare the adiabatic predictions obtained in the present work. The time-averaged results from the simulation will be presented to further demonstrate that the code yields realistic physical results and is valid for the present study. It is important to note that the time-averaged results were used as an initial solution for all unsteady simulations.

A. Problem Description

Chana and Jones [29] recorded experimental data in the Isentropic Light Piston Facility, which is a short-duration wind tunnel that allows full-sized high-pressure turbine stages to be tested. The inlet total pressure and inlet total temperature were reported at 4.6×10^5 Pa and 444 K, respectively, and these values were used to apply constant pressure and temperature profiles at the inlet of the vane domain. At the outlet, [29] specified static-pressure readings at the rotor exit at both the hub and casing, which were 1.428×10^5 Pa and 1.435×10^5 Pa respectively, and these values were used as the extremities of a linear pressure profile at the outlet of the rotor domain. The rotor speed was set at 9500 rpm [29].

It is important to note that the turbine stage geometry of [29] was approximated in the present study. In [29], a stator with 32 vanes was used, and the rotor consisted of 60 blades. In the present study, the

geometry has been scaled so that 30 vanes and 60 blades are modeled, allowing only one vane and two blades to be used to represent the turbine stage, as opposed to modeling 8 vanes and 15 blades. The geometric model for the turbine stage in [29] was obtained through inference by extracting the basic shape of the airfoils and gas path from figures available in the open literature. Using this information, the geometry was scaled to 30 vanes, using tools available in the industry. In addition, the tip clearance was not known and it was assumed to be 1.2 mm, which is the size of the gap used in a similar study in [30,31]. In addition, the location of the inlet and the outlet of the turbine stage were unknown and had to be assumed.

B. Grid Independence

Grid independence tests were first conducted before obtaining any results. Constant total pressure and total temperature distributions were defined at the inlet of the NGV domain, with a linear static-pressure distribution at the rotor exit, as already described. Four steady-state runs were performed using the exact conditions of the experimental study, but each with different grid counts. All grids consisted of a node count of 49, with an additional 16 nodes in the tip clearance region in the radial direction. The node counts in the axial and circumferential directions were varied to determine the coarsest mesh that could be used while yielding similar results to finer meshes. The total node counts for the four cases were 313,698, 534,934, 657,874, and 742,938 nodes, respectively.

To show the grid independence in two different directions, the static-pressure profile at the exit of the NGV (Fig. 4) was recorded with the isentropic Mach number distribution on the vane airfoil suction surface at midspan (Fig. 5). Figure 4 shows a linear static-pressure distribution at the NGV exit, which is expected, because a linear pressure distribution was defined at the outlet of the rotor exit. Figure 5 shows the variation of the isentropic Mach number in the axial direction on the vane airfoil suction surface. The differences in the results occur in the downstream region, which coincides with the development of the suction-side wakes. Finally, the static-pressure profile at the midspan of the tip clearance region and along the blade tip camber line is shown in Fig. 6.

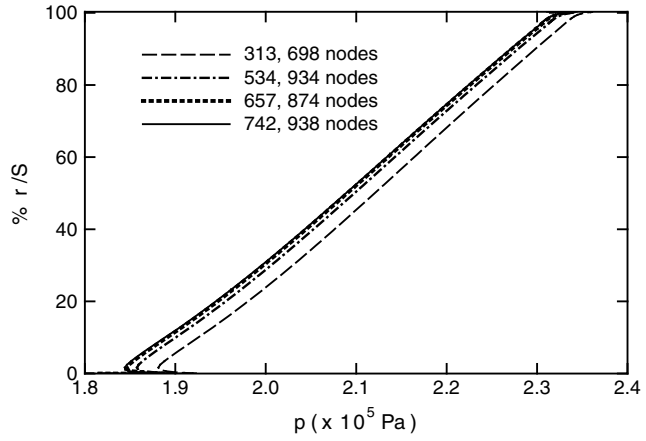

Fig. 4 Static pressure profiles at the exit of the NGV obtained from grids with different node counts.

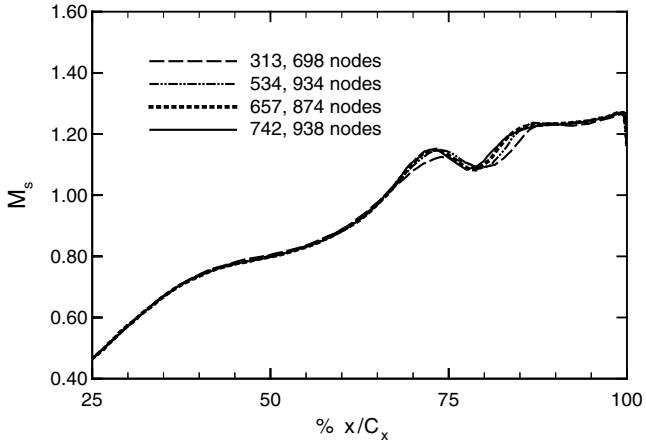

Fig. 5 Isentropic Mach number distribution on the vane airfoil suction surface at midspan obtained from grids with different node counts.

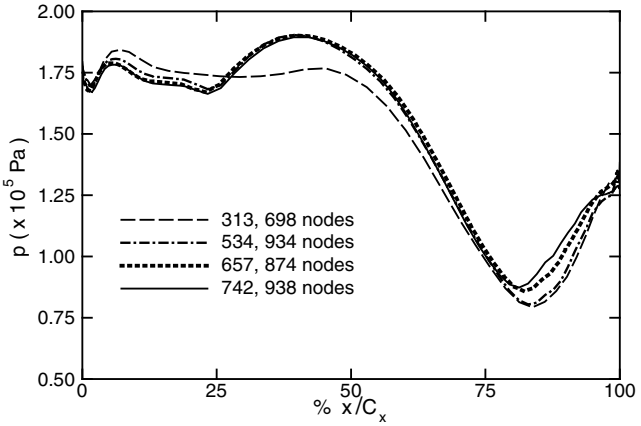

Fig. 6 Static pressure profiles at the midspan of the tip clearance region along the camber line of the blade tip obtained from grids with different node counts.

It can be seen in these figures that the coarsest mesh underpredicted the results from much finer meshes and that predictions obtained with 657,874 nodes and 742,938 nodes yielded similar results. It should be noted that in Fig. 6, the percent difference between the static-pressure values above $x/C_x = 75\%$ is less than 5%. Therefore, a grid count of 657,874 nodes was used for all cases in the present study.

C. Comparison with Experimental Results

Convergence for the time-averaged simulations was determined by the mass flow rate, total pressure, static pressure, and total temperature at the NGV and rotor inlets and exits. A summary of the final steady-state values for these parameters is given in Table 1. It should be noted that all parameters, except the mass flow rates, are the mass-averaged values. From Table 1, it can be seen that the flow shows typical behavior for that found in turbines. First, it was observed that the mass flow rate is conserved from the NGV inlet to the rotor exit for both simulations. In addition, there is an evident drop in the stagnation pressure and temperature across the rotor, which is due to the turbine expansion process and the extraction of kinetic energy from the fluid. On the other hand, there is very little drop in the total pressure across the NGV, which is expected, because

Table 1 Steady-state values for the convergence parameters for the baseline case

Location	Parameter	Final steady-state value
NGV inlet	W, kg/s	11.810
	$p_o(\times 10^5$ Pa)	4.599[a]
	T_o, K	444.294[a]
NGV exit	W, kg/s	11.816
	$p_o(\times 10^5$ Pa)	4.329
	$p(\times 10^5$ Pa)	2.094
	T_o, K	444.322
Rotor Inlet	W, kg/s	11.815
	$p_o(\times 10^5$ Pa)	4.329
	T_o, K	444.322
Rotor exit	W, kg/s	11.793
	$p_o(\times 10^5$ Pa)	1.646
	$p(\times 10^5$ Pa)	1.434[a]
	T_o, K	348.542

[a]Indicates values inputted as constants in the CFD solver.

Table 2 Comparison of the exit isentropic Mach numbers at the NGV exit

Study	Location	NGV exit isentropic Mach number
Chana and Jones [29]	Hub	1.034
	Casing	0.925
Nistar	Hub	1.191
	Casing	1.010

there is no work being extracted here. However, there is a drop in the static pressure, because the subsonic flow is being accelerated through the NGV as it guided smoothly to the rotor. Consequently, the flow is expanded across the NGV as well.

Predictions obtained with the Nistar were compared with experimental data to validate its use for the present study. The isentropic Mach numbers at both the hub and casing at the exit of the NGV are compared in Table 2 and show good agreement, with less than 15% difference. In both cases, the value of the isentropic Mach number is higher at the hub, which is expected, because the velocity at the casing is reduced, due to relative motion of the shroud. The difference in the values could be due to the fact that the NGV model was scaled to 30 vanes, whereas the NGV used in [29] consisted of 32 vanes. In addition, as mentioned before, the entire geometry for the both the NGV and rotor domains was obtained through inference of the information presented in [29].

In Fig. 7, the variation of the adiabatic-wall temperature on the shroud in the axial direction was compared. The experimental data were recorded at one row of gauges in the rotor passage. Because the location of the gauges was unknown, circumferentially averaged data from eight planes in the circumferential direction were obtained from the simulation results and used for comparison. The prediction is in very good agreement with the experimental data. Because there is no heat transfer in the simulation, the drop in the temperature in the axial direction is evident of the work extraction across the rotor. At the leading edge of the shroud, the total temperature is equal to 444 K, which is expected because there is no work extraction across the NGV because the domain is stationary. The amount of drop in the temperature is very comparable with the experimental data, and thus it was concluded that Nistar was appropriate for modeling the turbine stage in [29]. As a result, the time-averaged results were analyzed to study the time-averaged behavior of the tip leakage flow in the shroud region. Note that the results in the rotor domain are considered in the rotating reference frame.

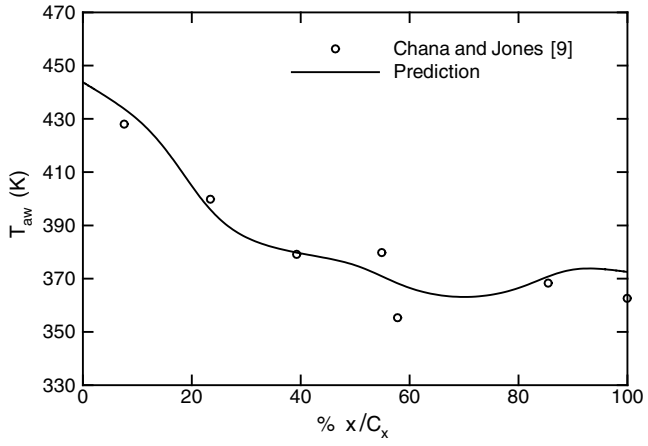

Fig. 7 Comparison of the circumferentially averaged adiabatic-wall temperature variation on the shroud in the axial direction.

IV. Results and Discussion

Figure 8 shows the typical flow pattern of the tip leakage flow as it enters the gap between the blade tip and shroud. As the leakage flow enters from the pressure side of the blade tip, a separation bubble forms at the blade tip, due to the sudden change in curvature of the blade surface. The leakage flow that is moving from the pressure side to the suction side dominates near the pressure side of the blade tip. On the suction side, the blade-passage flow originating from the pressure side of the adjacent blade (Fig. 9) enters the gap near the shroud. The combined effect of the relative motion of the shroud is from the suction side to the pressure side, and the passage flow causes a strong flow from the suction side to the pressure side near the shroud. As a result, the leakage flow that is moving from the pressure side to the suction side must negotiate the opposing flow near the shroud and must therefore move downward.

The relative x-, y-, and z-velocity profiles in the tip gap region at approximately $x/C_x = 48\%$ and on the camber line of the blade tip are presented in Figs. 10–12, respectively. The relative x velocity shown in Fig. 10 is, in fact, the axial component of the flow velocity, and an extremely steep velocity gradient can be observed at both the blade tip and shroud, where the relative x velocity is zero. The relative x velocity at the shroud is zero, which is expected, because the shroud's only movement is in the circumferential direction, and due to no-slip boundary conditions, the flow adjacent to the shroud should likewise move at the same velocity and in the same direction. A maximum of 222 m/s occurs at the middle of the gap, measuring only 1.2 mm, which is extremely high for such a small space.

It is important to study the relative y-velocity profile in the tip gap region (Fig. 11), because the y direction is essentially the circumferential direction, which is the direction of the leakage flow as well as the shroud relative motion. As expected, the velocity is zero at the blade tip and continues to increase in the radial direction, due to the presence of the leakage flow. However, almost

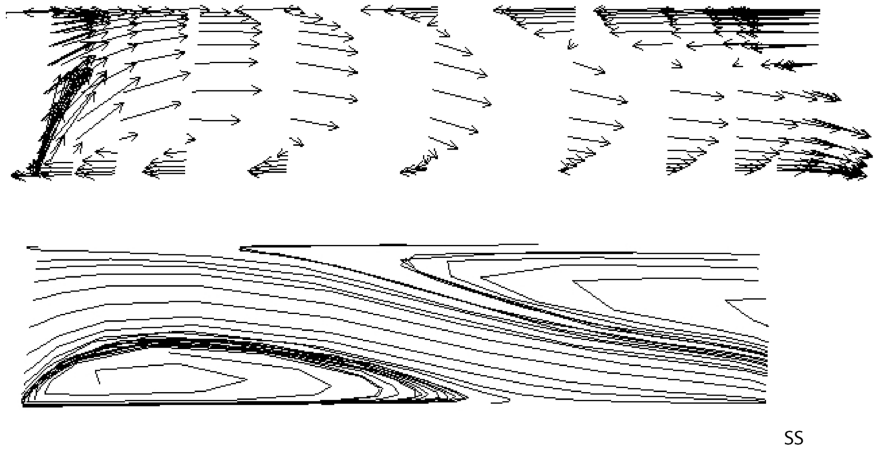

Fig. 8 Tip leakage structure inside tip leakage region as described by a) vectors and b) streamlines.

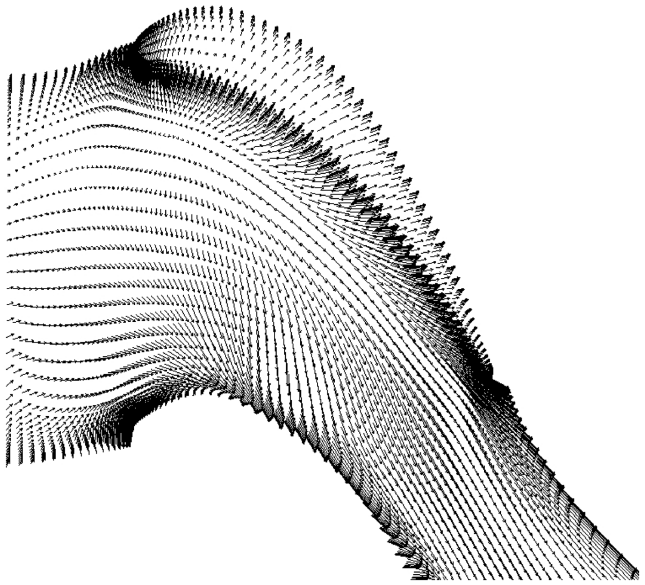

Fig. 9 Velocity vectors in the rotor passage entering the tip gap region.

immediately, the velocity jumps to −80 m/s just above the blade tip. The negative sign indicates flow moving from the suction side to the pressure side. The relative y velocity is negative until approximately $r/h = 8\%$, and this could represent the presence of the recirculation surrounding the separation bubble at this location. The velocity then

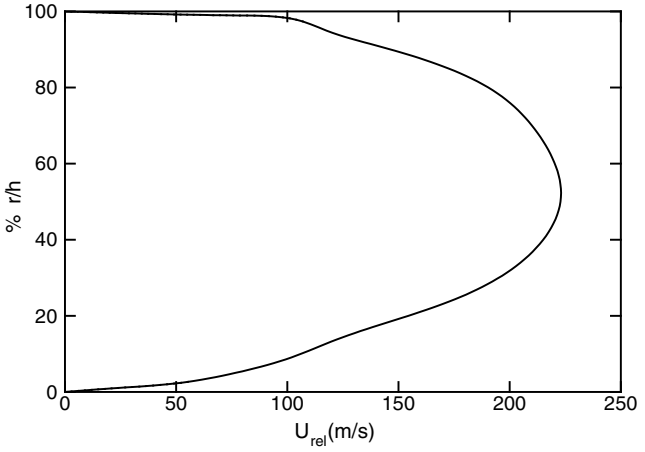

Fig. 10 Relative x-velocity profile in the tip clearance region at approximately $x/C_x = 48\%$ and on the camber line of the blade tip.

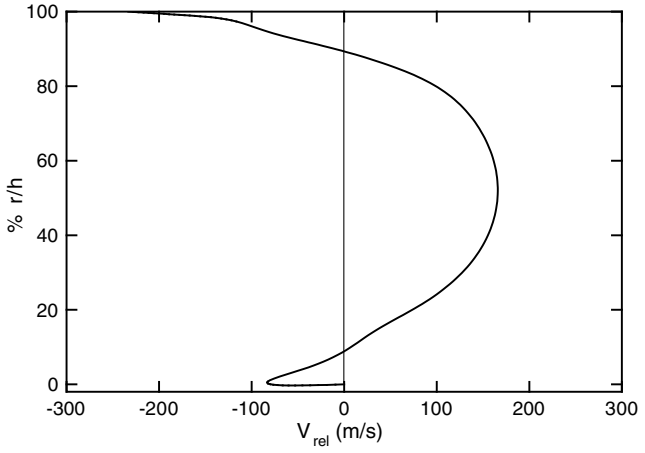

Fig. 11 Relative y-velocity profile in the tip clearance region at approximately $x/C_x = 48\%$ and on the camber line of the blade tip.

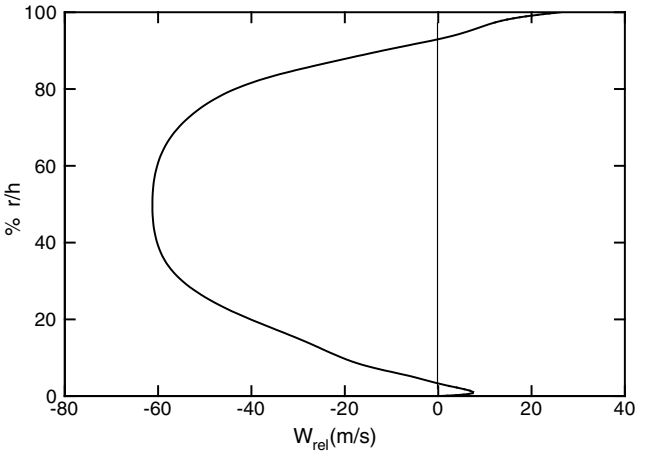

Fig. 12 Relative z-velocity profile in the tip clearance region at approximately $x/C_x = 48\%$ and on the camber line of the blade tip.

becomes positive from $r/h = 8$ to 86%, which shows the dominance of the leakage flow moving from the pressure side to the suction side of the blade tip. From $r/h = 86$ to 100%, the effect of the wall's relative motion becomes significant near the shroud, causing the flow velocity to change direction. As a result, a stagnation point develops, where the relative y velocity is zero at 90% r/h. This will cause a region of high pressure in the tip clearance region, rendering it susceptible to high heat transfer rates at this location.

The magnitude of the relative z velocity is relatively small compared with its x and y counterparts, as shown in Fig. 12. The direction of the radial component of relative velocity is mainly downward (negative), except near the blade tip and the shroud. The maximum absolute value is −60 m/s compared with 222 and 165 m/s for the relative x and y velocities, respectively. The smaller magnitude makes sense because the height of the tip gap region is so small, leaving little room for the flow to be maneuvered in the radial direction. Near the blade tip, it was observed that the relative z velocity is slightly positive or moving upward, which indicates the presence of recirculation from the separation bubble. In addition, the relative z velocity gradient is very steep near the shroud, and another stagnation point, for which the relative z velocity is zero, can be found at 92% r/h. This point indicates the intersection between the leakage flow and the flow caused by the relative motion of the shroud. Below 92% r/h, the flow is moving downward as the leakage flow maneuvers around the boundary-layer flow from the shroud. The change in the flow direction closer to the shroud indicates the presence of the boundary-layer flow, which has a slight upward motion, due to its interaction with the tip leakage flow.

Figure 13 shows the relative y velocity at different axial locations in the tip clearance region. Near the leading edge at $x/C_x = 5\%$, it can be seen that near the blade tip, the flow is moving from the suction side to the pressure side, indicating the presence of the separation bubble. Likewise, the flow near the shroud also moves opposite to the leakage flow, due to the casing relative motion. The leakage flow dominates in this area, attaining a maximum velocity of 316 m/s at 22% r/h. At $x/C_x = 48\%$, the same y-velocity profile as presented in Fig. 11 is shown for comparison. Near the trailing edge at $x/C_x = 95\%$, the velocity throughout the height of the tip clearance region is negative. This is indicative of the thickness of the airfoil being thinnest at the trailing edge. Thus, the crossflow originating from the passage flow dominates because there is little pressure drop across the blade tip in this area. There is still an influence from the leakage flow, however, which was observed at 22 to 50% r/h, where the y-velocity profile moves slightly toward the positive values.

Figure 14 shows the resultant relative Mach number profile in the tip clearance region at approximately $x/C_x = 48\%$ and on the camber line of the blade tip. A steep velocity gradient was observed at the blade tip, the flow just above the blade tip is moving at a relative Mach number of 0.2, and the blade tip is at zero relative velocity. The velocity remains steady at approximately Mach 0.2 until 5% r/h,

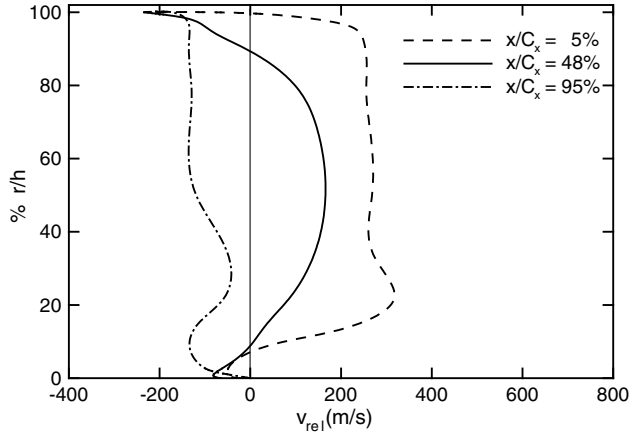

Fig. 13 Relative y-velocity profiles along the camber line at a) $x/C_x = 5\%$, b) $x/C_x = 48\%$, and c) $x/C_x = 95\%$.

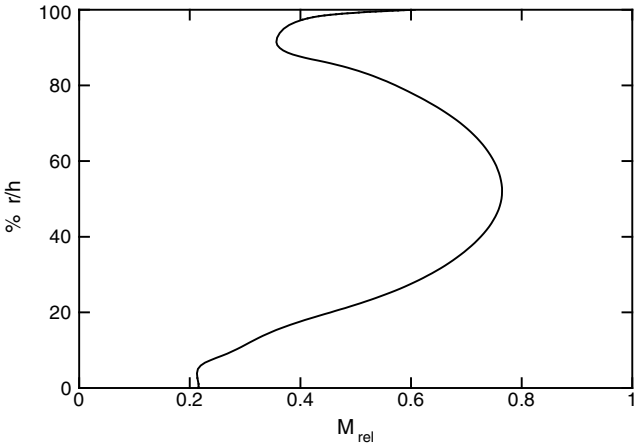

Fig. 14 Relative Mach number profile in the tip clearance region at approximately $x/C_x = 48\%$ and on the camber line of the blade tip.

indicating the presence of the separation bubble, which prevents the development of a parabolic velocity profile. From Fig. 12, it can be seen that the relative z velocity is positive or upward until approximately $5\% r/h$, which slightly obstructs the leakage flow which has a downward motion because it must negotiate the separation bubble at the blade tip and opposing boundary-layer flow at the shroud. Thus, the resultant Mach number profile shows a slight delay before developing into a parabolic shape from 5–92% r/h. Above 92% r/h, the effect of the shroud boundary layer becomes dominant. The motion of the shroud causes the flow adjacent to it to move from the suction side to the pressure side of the blade, which is in the opposite direction of the leakage flow. As a result, the relative y and z velocities become zero at approximately 92% r/h, as can be seen in Figs. 11 and 12, after which they increase once again. Also, the relative x velocity decreases rapidly to zero from 92–100% r/h, and so only the y and z velocities contribute to the resultant Mach number, which explains why the Mach number increases near the shroud.

The static-temperature profile in the tip clearance region at approximately $x/C_x = 48\%$ and on the camber line of the blade tip is presented in Fig. 15. At the blade tip, an adiabatic-wall temperature of 382 K was found, and a temperature of 373 K was found at the shroud. The temperature profile follows a trend opposite to that of the relative Mach number in Fig. 14, as expected. As the flow accelerates, the kinetic energy increases, and so the static temperature must decrease, due to conservation of energy. The opposite trend occurs if the flow decelerates, whereby the static temperature increases, due to conservation of energy. The static temperature reaches a minimum of 346 K at the midspan of the tip

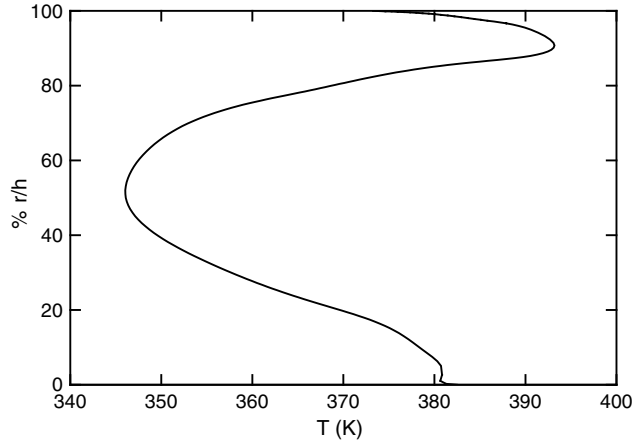

Fig. 15 Static-temperature profile in the tip clearance region at approximately $x/C_x = 48\%$ and on the camber line of the blade tip.

clearance region (50% r/h) and increases to a maximum of 390 K at 05% r/h.

Next, the flow behavior in the axial direction will be investigated. Figure 16 shows the relative Mach number variation at the midspan of the clearance region along the camber line of the blade tip. Near the leading edge, the relative Mach number decreases until $x/C_x = 25\%$, and this was attributed to the presence of the separation bubble, because it was observed that most of the leakage flow enters the tip clearance region near the leading edge. From $x/C_x = 25$ to 81%, the flow accelerates to a relative Mach number of 1.36, indicating that the flow is inside a recirculation region caused by the opposing flow changing direction inside the tip clearance region midspan. It is also important to note that in Figs. 10–12, the magnitudes of the velocity components at $x/C_x = 48\%$ are at their maximum values at midspan. Near the trailing edge, the tip leakage flow decelerates once again, indicating that the opposing flow from the suction side is dominant as it enters the tip clearance through the suction side.

The variation of the static temperature in the axial direction at the midspan of the tip clearance region along the camber line is shown in Fig. 17. As expected, the trend is opposite to the relative Mach number distribution shown in Fig. 16. The static temperature increases as the flow decelerates, due to obstruction caused by the separation bubble. Because of conservation of energy, the velocity is decreasing and so the kinetic energy is transformed into internal energy, thus increasing the static temperature. Once the leakage flow negotiates around the separation bubble at $x/C_x = 21\%$, it is able to accelerate until $x/C_x = 81\%$, thus decreasing the temperature of the flow as energy is transformed into kinetic energy. At the trailing edge, the leakage flow decelerates once again as it meets the opposing secondary crossflow from the adjacent blade passage. The

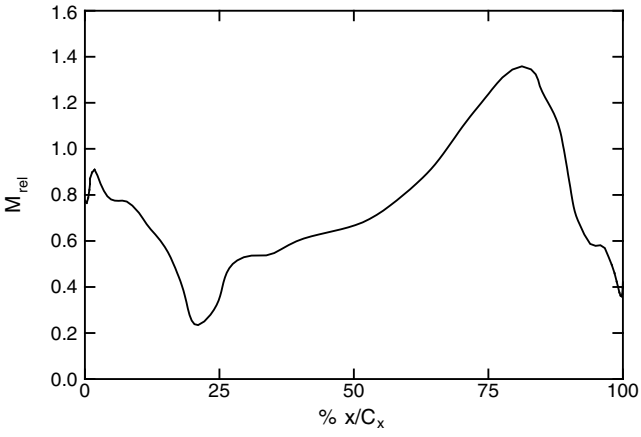

Fig. 16 Variation of the relative Mach number at the midspan of the tip clearance region along the camber line of the blade tip.

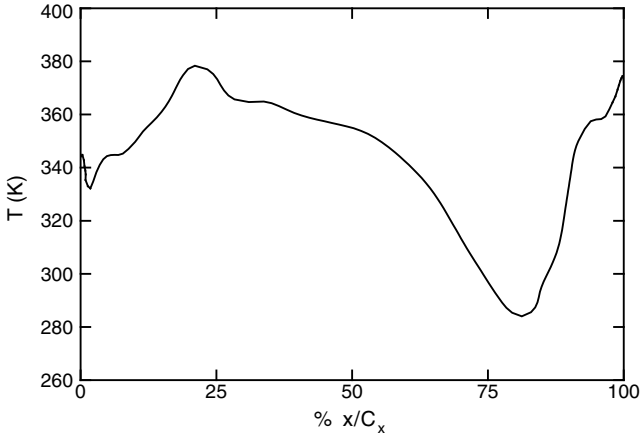

Fig. 17 Variation of the relative static temperature at the midspan of the tip clearance region along the camber line of the blade.

deceleration causes the internal energy to increase, thus raising static temperature near the trailing edge.

Figure 18 shows the mass flow rate entering the tip clearance region through the pressure side and exiting through the suction side at midspan. For the pressure-side curve, positive mass flow rates indicate flow entering the tip clearance region. For the suction-side curve, negative mass flow rates represent flow exiting the tip clearance region. It can be seen from this curve that the mass flow entering and exiting the tip leakage region is nearly identical at each axial location until $x/C_x = 50\%$, after which, more mass flow appears to be leaving than entering at a particular axial location. This is due to the fact that further downstream, the leakage flow does not cross over the blade tip at an angle perpendicular to the axial direction. Instead, the flow enters at an angle that depends on the shape of the airfoil and flow conditions. It can be seen from Fig. 18 that most of the leakage flow enters the tip clearance region at the leading edge, as expected. A maximum flow rate of $3.49 \times 10^{-5}\%$ enters and leaves the tip clearance region at the leading edge. Leakage flow continues to enter until $x/C_x = 77\%$, after which flow exits at both the suction side and the pressure side. This is due to the interaction of the leakage flow with the secondary crossflow causing the flow to wrap up into a recirculation zone near the trailing edge. The flow rotates in a plane parallel to the blade tip, and near the trailing edge, the airfoil thickness is small. As a result, the rotating flow will exit through both the pressure side and suction side near the trailing edge.

To examine the effect of the leakage flow on the shroud, the static-pressure and adiabatic-wall-temperature contours are presented in Figs. 19 and 20. The static pressure and adiabatic-wall temperature on the shroud reflect the flow behavior, which is described throughout this paper. From the pressure contours in Fig. 19, it can be seen that there is a low-pressure region near the trailing edge in the tip clearance region. This is indicative of the recirculation region already mentioned, which develops due to the interaction of the tip leakage flow with the secondary crossflow. In the rotor passage area, a pressure gradient can be observed spanning from the pressure side of the airfoil to the suction side of the adjacent blade at the throat area, which is the smallest area of the converging-diverging nozzle. As a result of this pressure gradient, secondary crossflow develops that moves from the pressure side of the airfoil to the suction side of the adjacent blade. However, a high-pressure region was found near the suction side at the throat area and was attributed to the interaction of the tip leakage flow with the secondary crossflow. As a result, another small recirculation zone appears in the rotor passage.

From Fig. 20, it can be seen that at the inlet of the shroud, the adiabatic-wall temperature is nearly equal to the total temperature of the turbine stage. This is expected, because no work was extracted from the NGV. High adiabatic-wall temperatures were observed at the leading edge of the blade tip. These high temperatures occur due to the flow deceleration that occurs as the flow from the vane strikes the blade tip's leading edge. In the tip clearance region, the adiabatic-wall temperature decreases from the leading edge to the trailing edge, indicating that work is being extracted from the rotor. In the rotor passage area, the adiabatic-wall temperature decreases in the

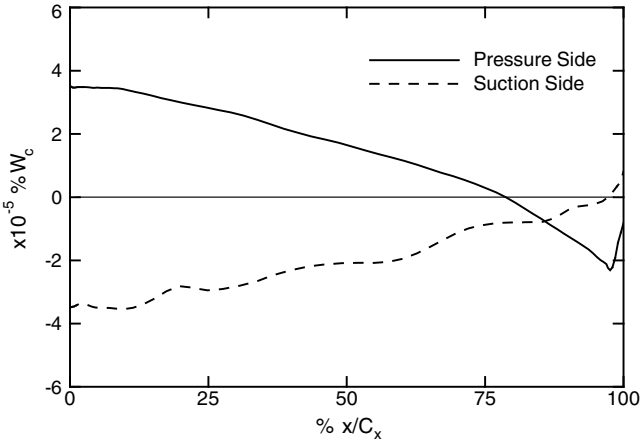

Fig. 18 Comparison of mass flow rates at the pressure side and suction sides of the tip clearance region at midspan.

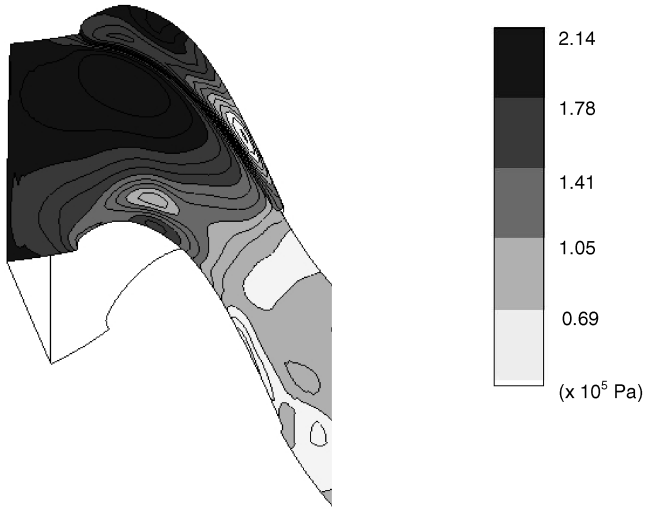

Fig. 19 Static-pressure contours on the shroud for steady simulation of the baseline case.

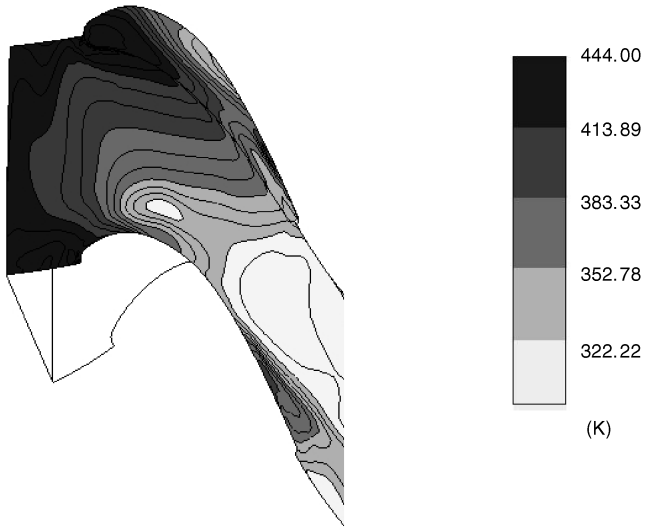

Fig. 20 Adiabatic-wall-temperature contours on the shroud for steady simulation of the baseline case.

circumferential direction along the throat area from the pressure side of the airfoil to the suction side of the adjacent blade. A region of low adiabatic-wall temperature develops in the passage area, which coincides with the recirculation zone already mentioned. The kinetic energy in the recirculation zone increases, which decreases the internal energy of the flow, due to conservation of energy.

V. Conclusions

In the present study, time-averaged and time-accurate simulations were performed to numerically study the tip leakage flow behavior using a 3-D Reynolds-averaged Navier–Stokes finite volume code. Results from the time-averaged simulation of the baseline case showed leakage flow entering the tip clearance region at the pressure side of the blade, causing the development of a separation bubble at this location. The separation bubble develops due to the sudden change in curvature as the leakage flow moves upward to negotiate the airfoil as it enters the tip clearance region. Near the pressure side of the tip clearance region and near the blade tip on the suction side, the leakage flow is dominant, whereas opposing flows entering through the suction side dominate near the shroud and at the suction side. This opposing flow is the combined effect of the shroud relative motion and the crossflow originating from the adjacent blade passage on the suction side. As a result, the circumferential and radial velocity profiles show regions of zero velocity in the tip clearance region.

The static pressure and adiabatic-wall temperature on the shroud were also obtained from the time-averaged solution. Another small recirculation region was observed above the rotor passage and was attributed to the blade-passage crossflow interacting with the high-pressure region found at the suction side of the blade. This high-pressure region is caused by the combined effect of the crossflow with the shroud boundary-layer flow interacting with the tip leakage flow inside the tip clearance region. In addition, the adiabatic-wall temperature decreases from the leading edge to the trailing edge in the tip clearance region, indicating the effect of the turbine expansion process and the extraction of kinetic energy from the fluid. High adiabatic-wall temperatures were found at the leading edge of the blade tip, which indicates that high heat transfer rates will occur in this region. These high temperatures were attributed to the flow deceleration that occurs as the flow from the vane strikes the blade tip's leading edge.

Acknowledgment

The authors would like to thank Pratt and Whitney Canada for sponsoring and providing financial support for this project.

References

[1] Allen, H. W., and Kofskey, M. G., "Visualization Study of Secondary Flows in Turbine Rotor Tip Regions," NACA TN 3519, 1955.

[2] Booth, T. C., Dodge, P. R., and Hepworth, H. K., "Rotor-Tip Leakage, Part 1: Basic Methodology," *Journal of Engineering for Power*, Vol. 104, No. 1, 1982, pp. 154–161.

[3] Wadia, A. R., and Booth, T. C., "Rotor-Tip Leakage, Part 2: Design Optimization Through Viscous Analysis and Experiment," *Journal of Engineering for Power*, Vol. 104, 1982, pp. 162–169.

[4] Yamamoto, A., Matsunuma, T., Ikeuchi, K., and Outa, E., "Unsteady Endwall/Tip-Clearance Flows and Losses Due to Turbine Rotor-Stator Interaction," American Society of Mechanical Engineers Paper 94-GT-461, 1994.

[5] Nikolos, I. K., Douvikas, D. I., and Papailiou, K. D., "Theoretical Modeling of Relative Wall Motion Effects in Tip Leakage Flow," American Society of Mechanical Engineers Paper 95-GT-88, 1995.

[6] Ristic, D., Lakshminarayana, B., and Chu, S., "Three-Dimensional Flow Field Downstream of an Axial Flow Turbine Rotor," AIAA Paper 98-3572, 1998.

[7] Xiao, X., McCarter, A. A., and Lakshminarayana, B., "Tip Clearance Effects in a Turbine Rotor, Part 1: Pressure Field and Loss," *Journal of Turbomachinery*, Vol. 123, No. 2, 2001, pp. 296–304. doi:10.1115/1.1368365

[8] McCarter, A. A., Xiao, X., and Lakshminarayana, B., "Tip Clearance Effects in a Turbine Rotor, Part 2: Velocity Field and Flow Physics," *Journal of Turbomachinery*, Vol. 123, No. 2, 2001, pp. 305–313. doi:10.1115/1.1368880

[9] Tallman, J., and Lakshminarayana, B., "Numerical Simulation of Tip Leakage Flows in Axial Flow Turbines, with Emphasis on Flow Physics, Part 2: Effect of Outer Casing Relative Motion," *Journal of Turbomachinery*, Vol. 123, No. 2, 2001, pp. 324–333. doi:10.1115/1.1369113

[10] Hassanvand, M., Tao, W. S., Tai, F. G., and Qi, W. Z., "Unsteady Simulation and Investigation of Tip Leakage Flow Based on Dissipation Function," *Proceedings of the ASME Turbo Expo 2004*, Vol. 5A, American Society of Mechanical Engineers, New York, 2004, pp. 973–982.

[11] Lampart, P., Yershov, S., Rusanov, A., and Szymaniak, M., "Tip Leakage/Main Flow Interactions in Multi-Stage HP turbines with Short-Height Blading," *Proceedings of the ASME Turbo Expo 2004*, Vol. 5B, American Society of Mechanical Engineers, New York, 2004, pp. 1359–1367.

[12] Camci, C., Dey, D., and Kavurmacioglu, L., "Aerodynamics of Tip Leakage Flows Near Partial Squealer Rims in an Axial Flow Turbine Stage," *Journal of Turbomachinery*, Vol. 127, No. 1, 2005, pp. 14–24. doi:10.1115/1.1791279

[13] Green, B. R., Barter, J. W., Haldeman, C. W., and Dunn, Michael, G., "Averaged and Time-Dependent Aerodynamics of a High Pressure Turbine Blade Tip Cavity and Stationary Shroud: Comparison of Computational and Experimental Results," *Journal of Turbomachinery*, Vol. 127, No. 4, 2005, pp. 736–746. doi:10.1115/1.1934410

[14] Palafox, P., Oldfield, M. L. G., LaGraff, J. E., and Jones, T. V., "PIV Maps of Tip Leakage and Secondary Flow Fields on a Low Speed Turbine Blade Cascade with Moving Endwall," *Proceedings of the ASME Turbo Expo 2005*, Vol. 6A, American Society of Mechanical Engineers, New York, 2005, pp. 465–476.

[15] Rhee, D.-H., and Cho, H. H., "Local Heat/Mass Transfer Characteristics on a Rotating Blade with Flat Tip in a Low Speed Annular Cascade, Part 2: Tip and Shroud," *Proceedings of the ASME Turbo Expo 2005*, Vol. 3A, American Society of Mechanical Engineers, New York, 2005, pp. 639–651.

[16] Bindon, J. P., "Measurement and Formation of Tip Clearance Loss," *Journal of Turbomachinery*, Vol. 111, No. 3, 1989, pp. 257–263.

[17] Yaras, M., Yingkang, Z., and Sjolander, S. A., "Flow Field in the Tip Gap of a Planar Cascade of Turbine Blades," *Journal of Turbomachinery*, Vol. 111, No. 3, 1989, pp. 276–283.

[18] Yamamoto, A., "Endwall Flow/Loss Mechanisms in a Linear Turbine Cascade with Blade Tip Clearance," *Journal of Turbomachinery*, Vol. 111, No. 3, 1989, pp. 264–275.

[19] Moore, J., Moore, J. G., Henry, G. S., and Chaudhry, U., "Flow and Heat Transfer in Turbine Tip Gaps," *Journal of Turbomachinery*, Vol. 111, No. 3, 1989, pp. 301–309.

[20] Sjolander, S. A., and Cao, D., "Measurements of the Flow in an Idealized Turbine Tip Gap," *Journal of Turbomachinery*, Vol. 117, 1994, pp. 578–584.

[21] Tallman, J., and Lakshminarayana, B., "Numerical Simulation of Tip Leakage Flows in Axial Flow Turbines, With Emphasis on Flow Physics, Part 1: Effect of Tip Clearance Height," *Journal of Turbomachinery*, Vol. 123, No. 2, 2001, pp. 314–323. doi:10.1115/1.1368881.

[22] Azad, G. S., Han, J. C., Bunker, R. S., and Lee, C. P., "Effect of Squealer Geometry Arrangement on a Gas Turbine Blade Tip Heat Transfer," *Journal of Heat Transfer*, Vol. 124, No. 3, 2002, pp. 452–459. doi:10.1115/1.1471523

[23] Jin, P., and Goldstein, R. J., "Local Mass/Heat Transfer on Turbine Blade Near-Tip Surfaces," *Journal of Turbomachinery*, Vol. 125, No. 3, 2003, pp. 521–528. doi:10.1115/1.1554410

[24] Willinger, R., and Haselbacher, H., "Axial Turbine Tip-Leakage Losses at Off-Design Incidences," *Proceedings of the ASME Turbo Expo 2004*, Vol. 5B, American Society of Mechanical Engineers, New York, 2004, pp. 993–1002.

[25] Metzger, D. E., Dunn, M. G., and Hah, C., "Turbine Tip and Shroud Heat Transfer," *Journal of Turbomachinery*, Vol. 113, No. 3, 1991, pp. 502–507.

[26] Ni, R. H., "A Multiple-Grid Scheme for Solving the Euler Equations," *AIAA Journal*, Vol. 20, No. 11, 1982, pp. 1565–1571.

[27] Ni, R. H., and Bogoian, J. C., "Prediction of 3D-Multistage Turbine Flow Field Using a Multiple-Grid Euler Solver," AIAA Paper 89-0203, 1989.

[28] Davis, R. L., Shang, T., Buteau, J., and Ni, R. H., "Prediction of 3-D Unsteady Flow in Multi-Stage Turbomachinery Using an Implicit Dual Time-Step Approach," AIAA Paper 96-2565, 1996.

[29] Chana, K. S., and Jones, T. V., "An Investigation on Turbine Tip and Shroud Heat Transfer," *Journal of Turbomachinery*, Vol. 125, No. 3, 2003, pp. 513–520. doi:10.1115/1.1575253

[30] Thorpe, S. J., Yoshino, S., Ainsworth, R. W., and Harvey, N. W., "An Investigation of the Heat Transfer and Static Pressure on the Over-Tip Casing Wall of an Axial Turbine Operating at Engine Representative Flow Conditions, Part 1: Time-Mean Results," *International Journal of Heat and Fluid Flow*, Vol. 25, No. 6, 2004, pp. 933–944. doi:10.1016/j.ijheatfluidflow.2004.02.027

[31] Thorpe, S. J., Yoshino, S., Ainsworth, R. W., and Harvey, N. W., "An Investigation of the Heat Transfer and Static Pressure on the Over-Tip Casing Wall of an Axial Turbine Operating at Engine Representative Flow Conditions, Part 2: Time-Resolved Results," *International Journal of Heat and Fluid Flow*, Vol. 25, No. 6, 2004, pp. 945–960. doi:10.1016/j.ijheatfluidflow.2004.02.028